Available online at www.sciencedirect.com
ScienceDirect
Trans. Nonferrous Met. Soc. China 32(2022) 1159−1168
Transactions of Nonferrous Metals Society of China
www.tnmsc.cn

Effect of duplex aging on microstructure and mechanical properties of near-β titanium alloy processed by isothermal multidirectional forging

Chang-jiang ZHANG[1], Xi JIANG[1], Zhi-dan LÜ[1], Hong FENG[1],
Shu-zhi ZHANG[1], Ying XU[2], Muhammad Dilawer HAYAT[2], Peng CAO[2]

1. College of Materials Science and Engineering, Taiyuan University of Technology, Taiyuan 030024, China;
2. Department of Chemical and Materials Engineering, the University of Auckland,
Private Bag 92019, Auckland 1142, New Zealand

Received 13 April 2021; accepted 24 September 2021

Abstract: The effects of sub-transus (α+β) annealing treatment (ST), followed by single aging (SA) or duplex aging (DA) on the microstructural evolution and mechanical properties of near-β Ti−4Al−1Sn−2Zr−5Mo−8V−2.5Cr (mass fraction, %) alloy were investigated using optical microscopy, scanning electron microscopy, and transmission electron microscopy. The results show that the finer secondary α phase precipitates in the alloy after DA than SA (e.g., 149 nm for SA and 69 nm for DA, both after ST at 720 °C). The main reason is that the pre-aging step (300 °C) in the DA process leads to the formation of intermediate ω phase nanoparticles, which assist in the nucleation of the acicular secondary α phase precipitates. In addition, the strength of the alloy after DA is higher than that of SA at the specific ST temperature. A good combination is achieved in the alloy subjected to ST at 750 °C, followed by DA (UTS: 1450 MPa, EL: 3.87%), which is due to the precipitation of nanoscale secondary α phase by DA. In conclusion, DA is a feasible process for this new near-β titanium alloy.

Key words: new near-β titanium alloy; multidirectional forging; annealing treatment; duplex aging; ω-assisted α nucleation; microstructure; mechanical properties

1 Introduction

Recently, near-β titanium alloys have become increasingly attractive for aerospace structural application, owing to their excellent mechanical properties such as superior specific strength, excellent toughness, and high heat resistance [1−3]. Heat treatment of near-β titanium alloys in either β or α+β phase region is adopted to tune the amount and morphology of the primary α (α_p) phase [4,5]. It is worth mentioning that, the alloys achieve better elongation after solution treatment in the α+β phase region because of the existence of the α_p phase [6,7]. The superior performance originates from the precipitation of finely dispersed secondary α (α_s) phase [8,9]. MANTRI et al [10] reported that the strength of a β titanium alloy TIMETAL® 21S (β-21S) increased to 1250 MPa and reasonably high tensile elongation of 8% could be achieved for the high strength. The refinement of α_s phase plays a critical role in strengthening β titanium alloy.

Apart from the conventional single aging (SA) process, aging processes involving an intermediate step have been developed in recent years. Previous studies have shown that the intermediate ω phase transforming from the metastable β phase serves as nucleation sites for the formation of α_s phase [11]. In a report of Ti-7333, DONG et al [12] observed that high-density intermediate ω phase precipitates

Corresponding author: Chang-jiang ZHANG, Tel/Fax: +86-351-6010022, E-mail: zhangchangjiang@tyut.edu.cn;
Peng CAO, Tel: +64-9-9236924, E-mail: p.cao@auckland.ac.nz
DOI: 10.1016/S1003-6326(22)65863-1

were formed during continuous heating to 600 °C. These ω precipitates promote the nucleation and precipitation of α_s phase in the later stage of continuous heating. Further, duplex aging (DA), consisting of a low-temperature pre-aging and a relatively high-temperature aging, has been found to improve the performance of titanium alloys. For instance, SANTHOSH et al [13] observed that the small size and dense precipitation of α phase after DA resulted in major improvement of higher strength. Overall, it is significantly meaningful to explore the effect of the microstructural evolution in DA on the mechanical properties of titanium alloys.

Ti−4Al−1Sn−2Zr−5Mo−8V−2.5Cr alloy is a newly-developed near-β titanium alloy. The hot deformation behavior and microstructural evolution of this alloy were investigated in our previous papers [14,15]. However, the investigation into heat treatment of this alloy is still lacking. In particular, the DA treatment mechanism has not been well understood. In this study, we conducted the sub-transus annealing treatment (ST) in the α+β region, followed by two different aging regimes (SA and DA) after multidirectional forging. The role of DA treatment in the nanoscale α_s phase by ω-assisted nucleation of new near-β Ti−4Al−1Sn−2Zr−5Mo−8V−2.5Cr alloy was analyzed. The phase transition sequence during aging process was represented by a schematic diagram. The mechanical properties of the alloy after SA and DA treatment were compared and the strength mechanism was discussed.

2 Experimental

The starting material used in this research was an as-forged Ti−4Al−1Sn−2Zr−5Mo−8V−2.5Cr (wt.%) alloy bar. We previously identified the β/α transformation temperature to be approximately 800 °C [14,15]. The multidirectional forging processes were reported elsewhere [15] and schematically shown in Fig. 1. After forging, the microstructure consists of intergranular α phase and β grains, as shown in Fig. 2. This microstructure was the starting point for the microstructural evolution study in this work.

The as-forged samples were firstly annealed in the α+β phase region at 720−780 °C for 0.5 h, followed by air cooling. After that, we applied two

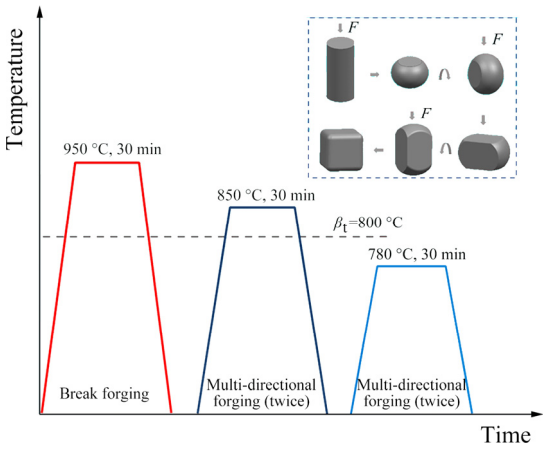

Fig. 1 Schematic of multi-directional forging process at deformation rate of 0.01 s^{-1} [15]

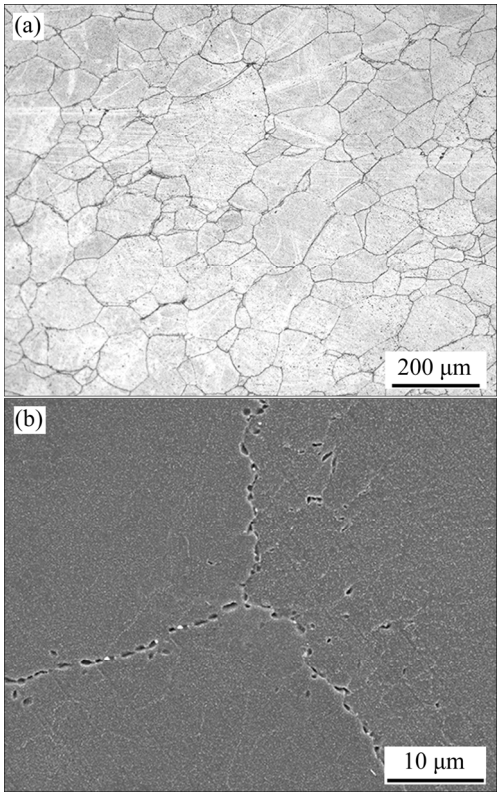

Fig. 2 Microstructures of multi-directionally forged sample: (a) OM image; (b) SEM image

different aging treatments. The first group of specimens was aged at 560 °C for 1 h (SA), followed by air cooling (STSA). For the second group of specimens, a pre-aging treatment was performed at 300 °C for 24 h, followed by air cooling to room temperature (hereafter marked as STPA). After the pre-aging, the specimens were re-heated to 560 °C for 1 h, followed by air cooling. This heat treatment process was designated as STDA hereafter.

Microstructure characterizations were carried out on a TESCAN MIRA3LMH scanning electron microscope (SEM) and a JEOL JEM−F200 transmission electron microscope (TEM). The standard metallographic method was followed, and a modified Kroll's reagent (3 mL HF + 5 mL HNO_3 + 92 mL H_2O) was used to reveal grain structure. The TEM samples were prepared with a focused ion beam (FIB, FIB200, FEI) technique. Moreover, the width and volume fraction of α phase and the size of β grains were quantified using the image analysis software (Image-Pro Plus 6.0). In order to acquire the mechanical property data of the current alloy, we conducted the tensile tests on an Instron 5500R testing machine at room temperature with a constant crosshead speed of 0.5 mm/min. The tensile samples (total length: 60 mm) with the size of gauge length part being 18 mm × 4 mm × 2 mm were prepared by electron discharge method, and their surfaces were polished with 80−2000 grid SiC paper. The tensile test was repeated in the same condition three times to obtain more accurate results.

3 Results and discussion

3.1 ST samples

The representative microstructures of the samples after ST at 720−780 °C are shown in Fig. 3. Figure 3 shows that the microstructures are highly sensitive to the heat treatment temperature by summarizing the average size of β grains and the volume fraction of the α_p phase shown in Fig. 4. It can be found from Figs. 3(a, b, c) and Fig. 4(a) that, the average diameter of the β grains increases from 104 to 123 μm with the ST temperature increasing from 720 to 780 °C. Meanwhile, the volume fraction of the α_p phase sharply decreases from 27% to 2%, as shown in Fig. 4(b). In addition, only trace amounts of α_p phases are distributed at the grain boundaries after treatment at 780 °C in Fig. 3(f). For the near-β titanium alloys, the driving force for the β-to-α transformation mainly depends on the thermodynamic stability of the β phase [16]. As per the phase diagram, the volume fraction of the α_p phase decreases with increasing temperature. However, the α_p phase at grain boundary can suppress grain growth [17], and consequently, the size of β grains increases with decreasing the volume fraction of the α_p phase. Nevertheless, the β grain size reported in this study when annealed in the α+β phase region is smaller than those of previously reported other alloys after being solutionized in the β phase region [18,19].

3.2 STPA samples

After the sub-transus annealing treatment, we investigated the effect of the pre-aging treatment at 300 °C for 1 h (i.e., without a secondary aging step and the samples are designated as STPA). The micrographs of the STPA samples are shown in Fig. 5. The average diameter of β grains and the volume fraction of α_p phase are also summarized in Fig. 4. Compared with the ST samples, the size of β grains and the volume fraction of α_p phase have no obvious change. However, SCHMIDT et al [20]

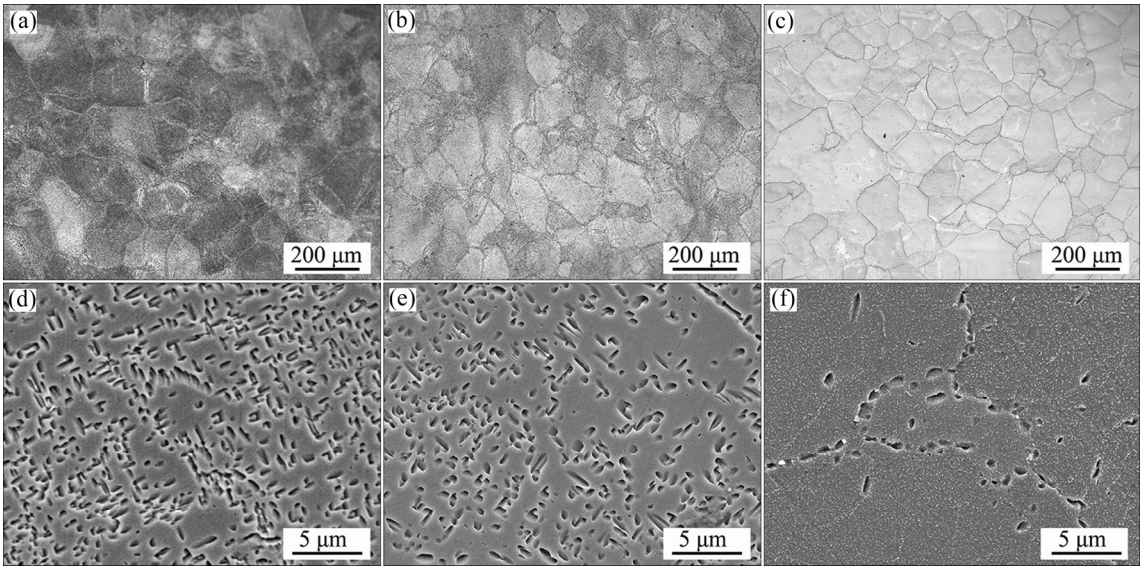

Fig. 3 Microstructures of alloy after ST at 720 °C (a, d), 750 °C (b, e) and 780 °C (c, f) for 0.5 h

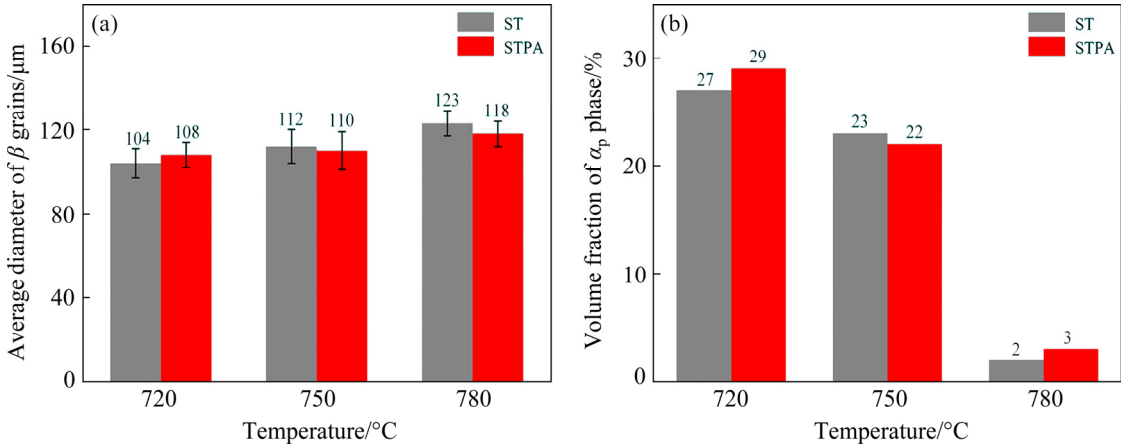

Fig. 4 Average diameter of β grains (a) and volume fraction of α_p phase (b) after ST and STPA

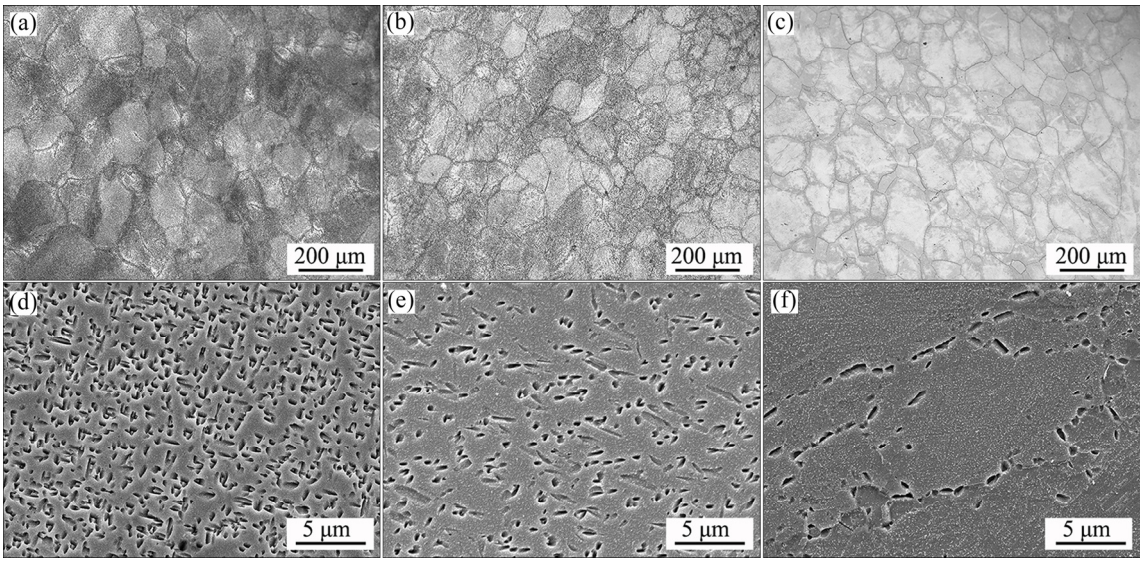

Fig. 5 Microstructures of samples subjected to pre-aging at 300 °C for 24 h after ST at different temperatures: (a, d) 720 °C; (b, e) 750 °C; (c, f) 780 °C

suggested that the pre-aging temperature affects the precipitation of α phase and found that α phase was uniformly distributed on the β' precursors after low-temperature pre-aging. FROES et al [21] reported that the ellipsoidal ω phase can be precipitated in a metastable β titanium alloy (Beta III) after long-time low-temperature aging.

3.3 STSA samples

SEM micrographs of samples after the ST followed by aging at 560 °C for 1 h are shown in Fig. 6. Nanometer-scale acicular α_s phase particles have emerged from the β matrix after aging at 560 °C. The volume fraction and size of these α_s particles are strongly influenced by the prior ST temperature. As shown in Fig. 7, the volume fraction of α_s phase increases from 42% to 75% and the average width decreases from 149 to 43 nm with increasing the ST temperature from 720 to 780 °C. The presence of α_p phase means that more β-stabilizing elements dissolve in the residual β phase, thus improving its stability [22]. At the ST temperature of 720 °C, the volume fraction of α_p phase is high, and therefore the residual β phase is very stable. Accordingly, the α_s phase precipitates are difficult to nucleate during the subsequent aging process. On the other hand, if the alloy is annealed at a high temperature, e.g., 780 °C, the residual β is less stable and therefore the α_s precipitates are more ready to nucleate. In general, the more the nucleation is, the finer the resulting precipitates are.

Hence, the smallest size of α_s precipitates is observed in the sample after the ST at 780 °C.

3.4 STDA samples

Figure 8 presents the microstructures of the STDA samples. It is clear that the evolution of the α_s precipitates of STDA samples presents a similar trend to that of the STSA samples. The volume fraction and the average width of α_s phase are also illustrated in Fig. 7. In comparison with the STSA samples, the average width of the α_s precipitates is smaller in the STDA samples. Concomitantly, the volume fraction of the α_s precipitates is greater in the STDA samples. Particularly, there is a significant difference in the width between the STSA and STDA samples at the ST temperature of 720 °C (149 nm for SA and 69 nm for DA). This may be related to the precipitation of intermediate phases during pre-aging.

For both STSA and STDA samples, the average width of the α_s particles decreases while the volume fraction increases with the prior ST temperature increasing (Fig. 7). Such results are consistent with other β alloys [23−25]. It is suggested that the fine and homogeneous distribution of α_s can be obtained during the aging process.

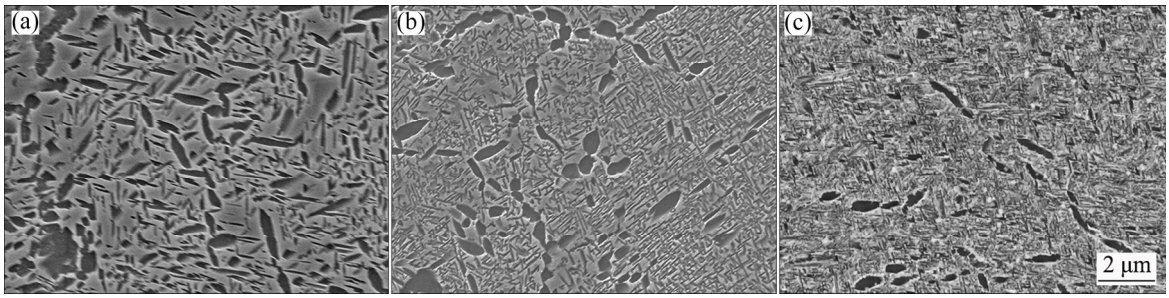

Fig. 6 Microstructures of alloys after ST at various temperatures followed by SA at 560 °C for 1 h: (a) 720 °C; (b) 750 °C; (c) 780 °C

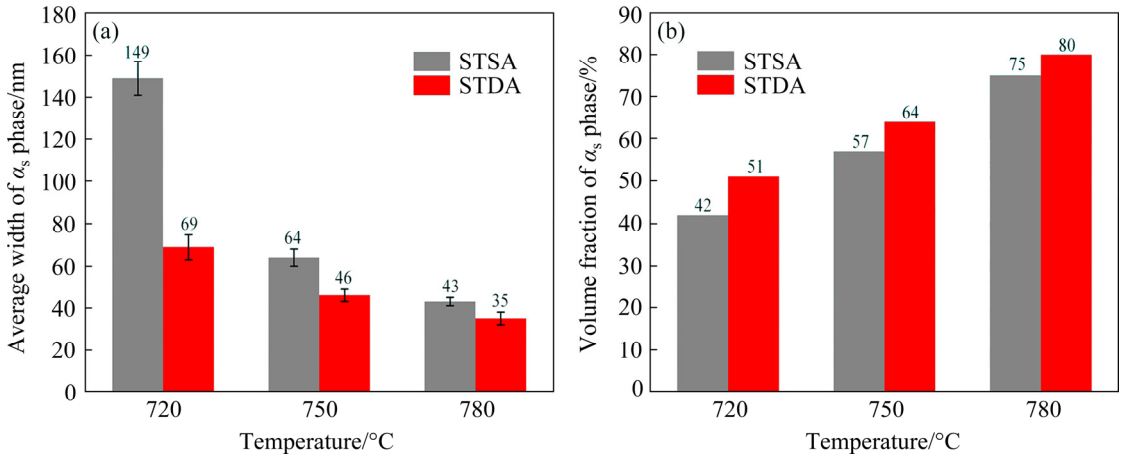

Fig. 7 Average width (a) and volume fraction (b) of α_s phase after STSA and STDA

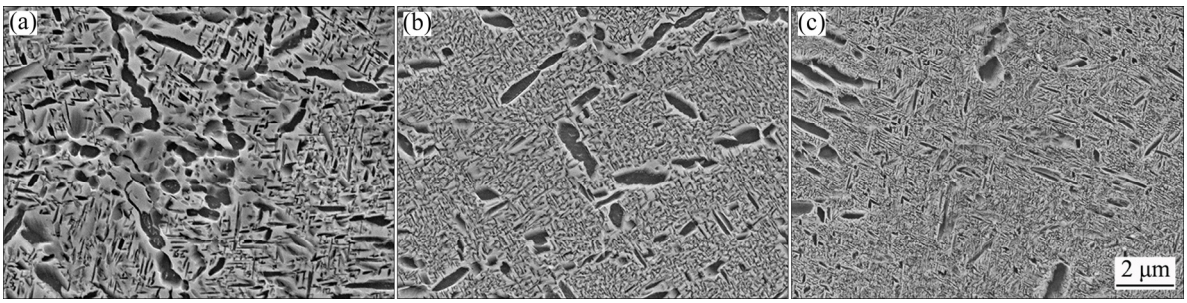

Fig. 8 Microstructures of alloys after ST at various temperatures followed by DA at (300 °C, 24 h) + (560 °C, 1 h): (a) 720 °C; (b) 750 °C; (c) 780 °C

3.5 TEM observations on STPA samples

3.5.1 STPA at 720 °C

In order to further investigate the phase transition behaviors during the pre-aging process, we examined these STPA samples by TEM. As shown in Figs. 9(a) and (b), few homogeneously distributed fine acicular α_s phase particles (light gray contrast) are precipitated in the β matrix after sub-transus annealing at 720 °C plus pre-aging. Meanwhile, the agglomeration zone of dark contrast ellipsoidal precipitates is observed in the bright contrast β matrix after ST at 720 °C followed by a pre-aging at 300 °C as shown in Fig. 9(c). Combined with morphology observation (Fig. 9(c)) and previous report [26], it can be inferred that the cluster is the agglomeration zone of ω phase, which could be the precursors for α_s phase precipitation. These precursors may have a positive effect on the nucleation and growth of the α_s phase during the aging process. We further conducted TEM observations of the pre-aged sample after sub-transus annealing at 780 °C to explain this phenomenon.

3.5.2 STPA at 780 °C

The dark-field TEM micrographs of the pre-aged sample after sub-transus annealing at 780 °C are shown in Figs. 10(a) and (b). Figure 10(c) shows its corresponding selected-area diffraction pattern of $[113]_\beta$ zone axis, which confirms that α phase and ω phase exist in β matrix simultaneously. This special type of electron diffraction pattern can also be found in previous report [27]. Figure 10(a) presents numerous ellipsoidal ω precipitates (bright contrast) distributed in the β matrix (darker contrast). Agglomerated precipitates (marked with a circle) are also observed and confirmed to be ω phase, and the precipitate size is approximately 10 nm. Figure 10(b) clearly shows that many embryonic α_s particles nucleated and grew by consuming the ω phase (one of these is marked with a dotted line in Fig. 10(b)).

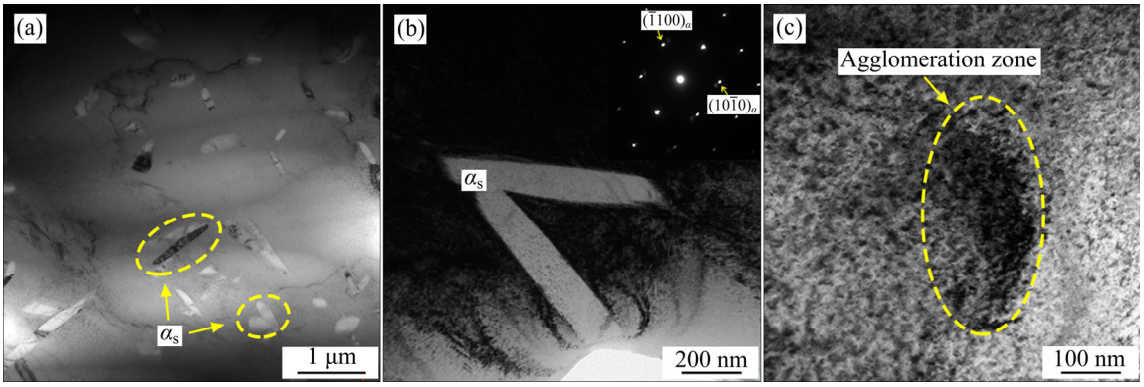

Fig. 9 TEM images of specimen after ST at 720 °C followed by pre-aging at 300 °C: (a) Bright-field TEM micrograph; (b) Fine acicular α_s phase at high magnification and its corresponding selected-area diffraction pattern of $[0001]_\alpha$ zone axis; (c) Bright-field TEM micrograph of agglomeration zone of precipitates

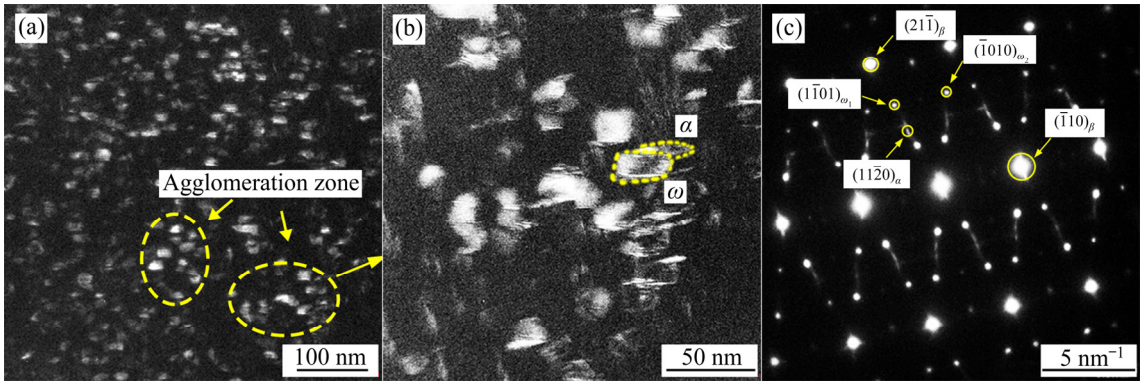

Fig. 10 TEM images of specimen after sub-transus annealing at 780 °C followed by pre-aging step at 300 °C: (a) Dark-field TEM micrograph; (b) High magnification of agglomeration zone in (a); (c) Corresponding selected-area diffraction pattern of $[113]_\beta$ zone axis

3.6 Model of phase transition of ω phase

We proposed phase transformations in the near-β titanium alloy, based on the observations made in this study and previous reports about the transformation process of ω phase to α phase [28,29]. Figure 11(a) shows a time−temperature−transformation (TTT)-like schematic diagram. The phase transformation curves are located between two temperatures. The low limit is a critical temperature for ω phase precipitation to occur. In other words, if the temperature is lower than this critical value, the formation of the intermediate ω phase will not occur. The upper limit is indeed the metastable β phase transus temperature. Figure 11(a) also schematically presents three stages (1, 2, 3) of phase transformation associated with the ω phase. The corresponding phase transformation sequence is $\beta + \alpha_p \rightarrow \beta + \alpha_p + \omega \rightarrow \beta + \alpha_p + \omega + \alpha_s$. Figures 11($b_1$, b_2, b_3) present how the phase transformation proceeds over time. At 300 °C (the pre-aging temperature), many nanoscale elliptical ω particles start to precipitate in the β matrix, and the ω aggregation zone is formed (Fig. 10(a) and Fig. 11(b_2)). At the final stage of the pre-aging step, as shown in Fig. 11(b_3), some ω phase particles start to transform into the α_s phase. That is, the α_s phase grows with ω phase as the nucleation point.

The schematic diagram of microstructure evolution of the alloy after the second-step aging (DA) treatment is shown in Fig. 11(b_4), where the intermediate phase ω has completely disappeared, and the acicular α_s precipitates grow over time.

3.7 Mechanical properties

Figure 12(a) compiles the tensile curves of typical samples. By comparing the STDA and STSA samples, it is found that the STDA samples have higher tensile strength but less sacrificial elongation than the respective STSA samples. This result is similar to the work by DONG et al [12]. The main reason is that the decrease of width and the increase of volume fraction lead to the increase of α/β interface, which in turn increases the slip resistance of dislocations.

The overall tensile strength (σ) can be approximated by a rule of mixtures and expressed as

$$\sigma = f_\beta \sigma_\beta + f_{\alpha_p} \sigma_{\alpha_p} + f_{\alpha_s} \sigma_{\alpha_s} \quad (1)$$

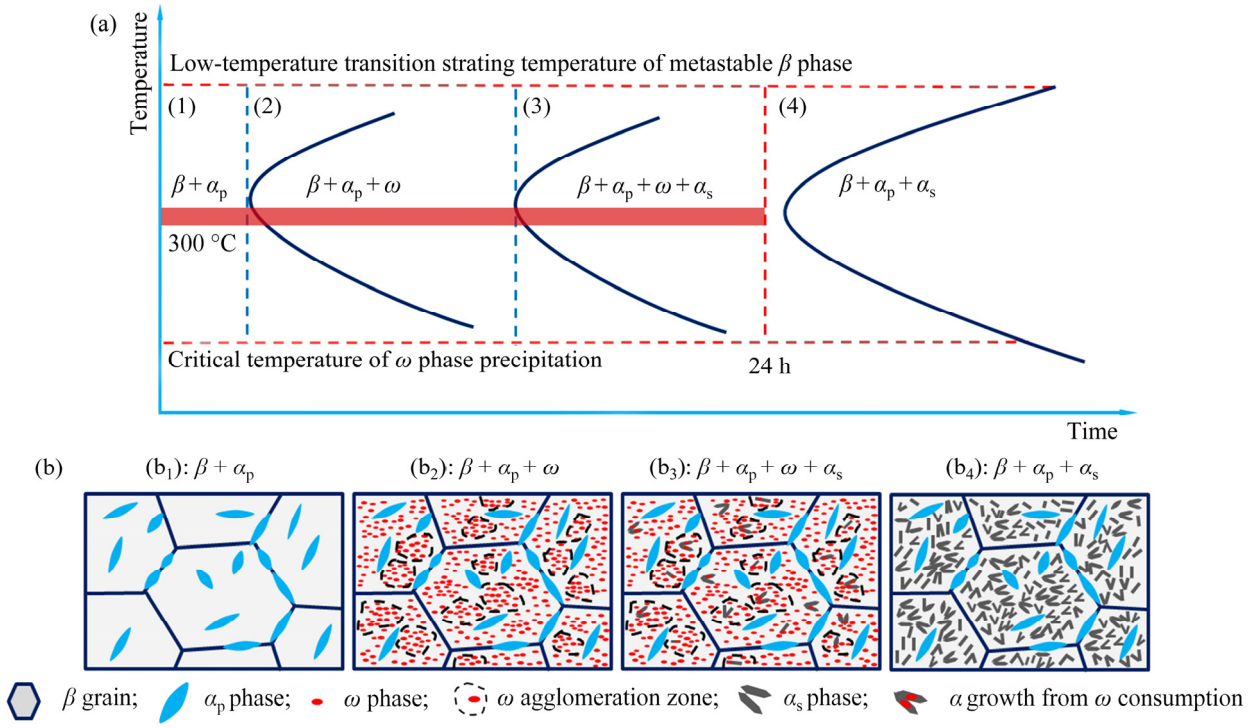

Fig. 11 ω phase transformation schematic diagrams during pre-aging at 300 °C for 24 h: (a) TTT diagram; (b_1–b_3) Three stages of phase transformation in (a), respectively; (b_4) Equilibrium microstructure of alloy after second-step aging treatment

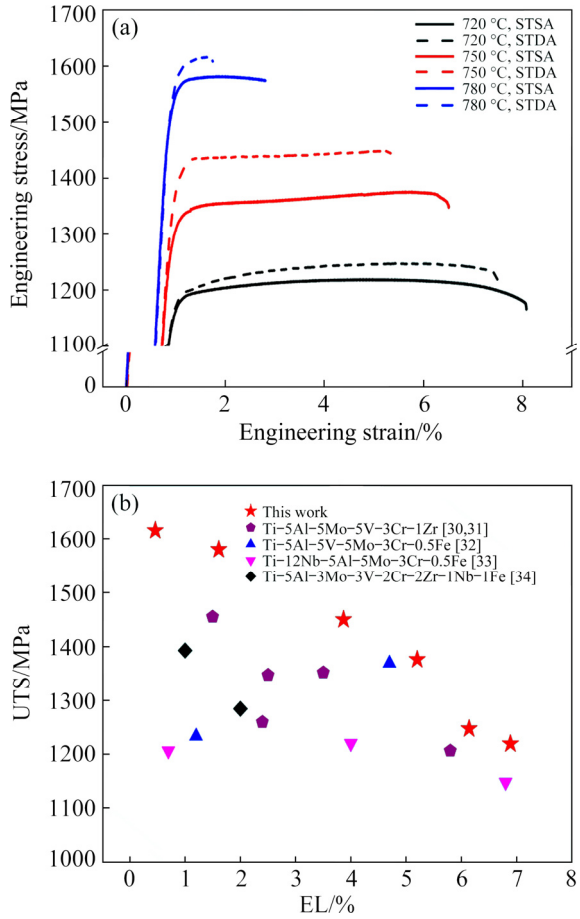

Fig. 12 Mechanical properties of Ti−4Al−1Sn−2Zr−5Mo−8V−2.5Cr alloy after STSA and STDA: (a) Typical tensile engineering stress−strain curves; (b) Comparison of mechanical properties of alloy in this work with other β titanium alloys (composition in wt.%) [30−34]

where σ is the strength, f is the fraction and subscripts β, α_p and α_s represent β, primary α and secondary α phases, respectively. Assuming the strength of the respective phase follows the well-known Hall−Petch relation, Eq. (1) can be rewritten as

$$\sigma \propto \frac{f_\beta}{\sqrt{d_\beta}} + \frac{f_{\alpha_p}}{\sqrt{d_{\alpha_p}}} + \frac{f_{\alpha_s}}{\sqrt{w_{\alpha_s}}} \quad (2)$$

where d is the average grain diameter (assuming equiaxed grains), and w_{α_s} is the width of the acicular α_s phase. The first two terms on the right-hand side of Eq. (2) do not change noticeably after DA, whilst the width of α_s phase decreases and the fraction of the α_s phase increases significantly. Therefore, the third term in Eq. (2) increases dramatically. Since the nature of the β phase and α_p phase remains essentially unchanged, the overall elongation does not sacrifice too much. Figure 12(b) compares our work with some previous reports [30−34], indicating that the current Ti−4Al−1Sn−2Zr−5Mo−8V−2.5Cr alloy shows better combination of strength of 1450 MPa and elongation of 3.87% after sub-transus annealing at 750 °C plus DA. We envision that this new alloy has a desirable development prospect.

4 Conclusions

(1) Increasing the sub-transus annealing temperature results in the decreased volume fraction of the α_p phase in the near-β Ti−4Al−1Sn−2Zr−5Mo−8V−2.5Cr alloy. Following sub-transus annealing, the aging process leads to the α_s precipitates. The volume fraction and size of the α_s phase are related to the prior sub-transus annealing temperature. Compared to SA, DA causes an increased volume fraction and a decreased width of the acicular α_s phase.

(2) Numerous dispersed isothermal ω phase particles emerge from the residual β matrix after the pre-aging step. These intermediate ω phase particles are deemed to be the precursors for the precipitation of the α_s phase during DA.

(3) Compared with SA, the alloy after DA has higher tensile strength and no obvious sacrifice of elongation. A good combination of strength of 1450 MPa and ductility of 3.87% was obtained in an alloy sample that was annealed at 750 °C, followed by DA at (300 °C, 24 h) + (560 °C, 1 h).

Acknowledgments

The authors are grateful for the financial supports from the Key Research and Development Program of Shanxi Province, China (Nos. 201903D421084, 201903D121056), and the National Natural Science Foundation of China (Nos. 52171122, 52071228, 51901151).

References

[1] BANERJEE D, WILLIAMS J C. Perspectives on titanium science and technology [J]. Acta Materialia, 2013, 61(3): 844−879.

[2] XU Xin, DONG Li-min, BA Hong-bo, ZHANG Zhi-qiang, YANG Rui. Hot deformation behavior and microstructural evolution of beta C titanium alloy in β phase field [J]. Transactions of Nonferrous Metals Society of China, 2016, 26: 2874−2882.

[3] DU Zhao-xin, HE Qi-wei, CHEN Rui-run, LIU Fei, ZHANG Jing-yong, YANG Fei, ZHAO Xue-ping, CUI Xiao-ming,

CHENG Jun. Rolling reduction-dependent deformation mechanisms and tensile properties in a β titanium alloy [J]. Journal of Materials Science & Technology, 2022, 104: 183−189.

[4] FAN Jiang-kun, LI Jin-shan, KOU Hong-chao, HUA Ke, TANG Bin, ZHANG Yu-dong. Influence of solution treatment on microstructure and mechanical properties of a near β titanium alloy Ti-7333 [J]. Materials & Design, 2015, 83: 499−507.

[5] ZHOU Zhong-bo, FEI Yue, LAI Min-jie, KOU Hong-chao, CHANG Hui, SHANG Guo-qiang, ZHU Zhi-shou, LI Jin-shan, ZHOU Lian. Microstructure and mechanical properties of new metastable β type titanium alloy [J]. Transactions of Nonferrous Metals Society of China, 2010, 20: 2253−2258.

[6] SHEKHAR S, SARKAR R, KAR S K, BHATTACHARJEE A. Effect of solution treatment and aging on microstructure and tensile properties of high strength β titanium alloy, Ti−5Al−5V−5Mo−3Cr [J]. Materials & Design, 2015, 66: 596−610.

[7] DU Zhao-xin, XIAO Shu-long, XU Li-juan, TIAN Jing, KONG Fan-tao, CHEN Yu-yong. Effect of heat treatment on microstructure and mechanical properties of a new β high strength titanium alloy [J]. Materials & Design, 2014, 55: 183−190.

[8] XU Sheng-hang, LIU Yong, LIU Bin, WANG Xin, CHEN Zhi-xing. Microstructural evolution and mechanical properties of Ti−5Al−5Mo−5V−3Cr alloy by heat treatment with continuous temperature gradient [J]. Transactions of Nonferrous Metals Society of China, 2018, 28: 273−281.

[9] WANG Zhen-yu, LIU Li-bin, WU Di, ZHANG Li-gang, WANG Wan-lin, ZHOU Ke-chao. α'' phase-assisted nucleation to obtain ultrafine α precipitates for designing high-strength near-β titanium alloys [J]. Transactions of Nonferrous Metals Society of China, 2020, 30: 2681−2696.

[10] MANTRI S A, CHOUDHURI D, BEHERA A, COTTON J D, KUMAR N, BANERJEE R. Influence of fine-scale alpha precipitation on the mechanical properties of the beta titanium alloy Beta-21S [J]. Metallurgical and Materials Transactions A, 2015, 46(7): 2803−2808.

[11] ZHENG Yu-feng, WILLIAMS R E A, SOSA J M, ALAM T, WANG Yun-zhi, BANERJEE R, FRASER H L. The indirect influence of the ω phase on the degree of refinement of distributions of the α phase in metastable β-titanium alloys [J]. Acta Materialia, 2016, 103: 165−173.

[12] DONG Rui-feng, LI Jin-shan, KOU Hong-chao, FAN Jiang-kun, ZHAO Yu-hong, HOU Hua, WU Li. ω-assisted refinement of α phase and its effect on the tensile properties of a near β titanium alloy [J]. Journal of Materials Science & Technology, 2020, 44: 24−30.

[13] SANTHOSH R, GEETHA M, SAXENA V K, NAGESWARA R M. Effect of duplex aging on microstructure and mechanical behavior of beta titanium alloy Ti−15V−3Cr−3Al−3Sn under unidirectional and cyclic loading conditions [J]. International Journal of Fatigue, 2015, 73: 88−97.

[14] WU Jie, LÜ Zhi-dan, ZHANG Chang-jiang, HAN Jian-chao, ZHANG Hong-zhou, ZHANG Shu-zhi, MUHAMMAD H, CAO Peng. Investigation of the deformation mechanism of a near β titanium alloy through isothermal compression [J]. Metals, 2017, 7(11): 498.

[15] LÜ Zhi-dan, ZHANG Chang-jiang, DU Zhao-xin, HAN Jian-chao, ZHANG Shu-zhi, YANG Fei, CHEN Yu-yong. Relationship between microstructure and tensile properties on a near-β titanium alloy after multidirectional forging and heat treatment [J]. Rare Metals, 2019, 38(4): 336−342.

[16] LÜ Zhi-dan, ZHANG Chang-jiang, FENG Hong, ZHANG Shu-zhi, HAN Jian-chao, JIA Yi, DU Zhao-xin, CHEN Yu-yong. Effect of heat treatment on microstructure and tensile properties of 2 vol.% TiC_p/near-β Ti composite processed by isothermal multidirectional forging [J]. Materials Science and Engineering A, 2019, 761: 138064.

[17] ZHU Yan-yan, CHEN Bo, TANG Hai-bo, CHENG Xu, WANG Hua-ming, LI Jia. Influence of heat treatments on microstructure and mechanical properties of laser additive manufacturing Ti−5Al−2Sn−2Zr−4Mo−4Cr titanium alloy [J]. Transactions of Nonferrous Metals Society of China, 2018, 28: 36−46.

[18] CHEN Wei, CAO Shuo, KOU Wen-juan, ZHANG Jin-yu, WANG Yue, ZHA You, PAN Yan, HU Qing-miao, SUN Qiao-yan, SUN Jun. Origin of the ductile-to-brittle transition of metastable β-titanium alloys: Self-hardening of ω-precipitates [J]. Acta Materialia, 2019, 170: 187−204.

[19] AHMED M, SAVVAKIN D G, IVASISHIN O M, PERELOMA E V. The effect of thermo-mechanical processing and ageing time on microstructure and mechanical properties of powder metallurgy near β titanium alloys [J]. Journal of Alloys and Compounds, 2017, 714: 610−618.

[20] SCHMIDT P, EL-CHAIKH A, CHRIST H J. Effect of duplex aging on the initiation and propagation of fatigue cracks in the solute-rich metastable β titanium alloy Ti 38-644 [J]. Metallurgical and Materials Transactions A, 2011, 42(9): 2652−2667.

[21] FROES F H, YOLTON C F, CAPENOS J M, WELLS M G H, WILLIAMS J C. The relationship between microstructure and age hardening response in the metastable beta titanium alloy Ti−11.5Mo−6Zr−4.5Sn (beta III) [J]. Metallurgical and Materials Transactions A, 1980, 11(1): 21−31.

[22] BOYNE A, WANG D, SHI R P, ZHENG Y, BEHERA A, NAG S, TILEY J S, FRASER H L, BANERJEE R, WANG Y. Pseudospinodal mechanism for fine α/β microstructures in β-Ti alloys [J]. Acta Materialia, 2014, 64: 188−197.

[23] MANTRI S A, CHOUDHURI D, ALAM T, VISWANATHAN G B, SOSA J M, FRASER H L, BANERJEE R. Tuning the scale of α precipitates in β-titanium alloys for achieving high strength [J]. Scripta Materialia, 2018, 154: 139−144.

[24] DU Zhao-xin, LIU Guo-long, LIU Fei, CHENG Jun, CHEN Yan-fei, CHEN Yun, HUANG Dong-nan, LIU Hui-min. Influence of pre-aging on microstructure and mechanical properties of coarse grained β titanium alloy [J]. Rare Metal Materials and Engineering, 2019, 48(3): 770−774. (in Chinese)

[25] REN Lei, XIAO Wen-long, HAN Wei-zhong, MA Chao-li, ZHOU Lian. Influence of duplex ageing on secondary α precipitates and mechanical properties of the near β-Ti alloy Ti-55531 [J]. Materials Characterization, 2018, 144: 1−8.

[26] LI Tong, KENT D, SHA Gang, STEPHENSON L T, CEGUERRA A V, RINGER S P, DARGUSCH M S, CAIRNEY J M. New insights into the phase transformations to isothermal ω and ω-assisted α in near β-Ti alloys [J]. Acta Materialia, 2016, 106: 353−366.

[27] NAG S, BANERJEE R, SRINIVASAN R, HWANG J Y, HARPER M, FRASER H L. ω-assisted nucleation and growth of α precipitates in the Ti−5Al−5Mo−5V−3Cr−0.5Fe β titanium alloy [J]. Acta Materialia, 2009, 57(7): 2136−2147.

[28] SHI Rong-pei, ZHENG Yu-feng, BANERJEE R, FRASER H L, WANG Yun-zhi. ω-assisted α nucleation in a metastable β titanium alloy [J]. Scripta Materialia, 2019, 171: 62−66.

[29] DUERIG T W, TERLINDE G T, WILLIAMS J C. Phase transformations and tensile properties of Ti−10V−2Fe−3Al [J]. Metallurgical Transactions A, 1980, 11(12): 1987−1998.

[30] WU Chuan, ZHAN Mei. Microstructural evolution, mechanical properties and fracture toughness of near β titanium alloy during different solution plus aging heat treatments [J]. Journal of Alloys and Compounds, 2019, 805: 1144−1160.

[31] WU Chuan, ZHAN Mei. Effect of solution plus aging heat treatment on microstructural evolution and mechanical properties of near-β titanium alloy [J]. Transactions of Nonferrous Metals Society of China, 2019, 29: 997−1006.

[32] SALVADOR C A F, OPINI V C, MELLO M G, CARAM R. Effects of double-aging heat-treatments on the microstructure and mechanical behavior of an Nb-modified Ti-5553 alloy [J]. Materials Science and Engineering A, 2019, 743: 716−725.

[33] OPINI V C, SALVADOR C A F, CAMPO K N, LOPES E S N, CHAVES R R, CARAM R. α phase precipitation and mechanical properties of Nb-modified Ti-5553 alloy [J]. Materials Science and Engineering A, 2016, 670: 112−121.

[34] SONG Bo, XIAO Wen-long, MA Chao-Li, ZHOU Lian. Influence of phase transformation kinetics on the microstructure and mechanical properties of near β titanium alloy [J]. Materials Characterization, 2019, 148: 224−232.

双级时效对等温多向锻造近β钛合金显微组织和力学性能的影响

张长江[1]，姜 燨[1]，吕智丹[1]，冯 弘[1]，张树志[1]，许 瑛[2], Muhammad Dilawer HAYAT[2]，曹 鹏[2]

1. 太原理工大学 材料科学与工程学院，太原 030024；

2. Department of Chemical and Materials Engineering, the University of Auckland, Private Bag 92019, Auckland 1142, New Zealand

摘 要：利用光学显微镜、扫描电子显微镜和透射电子显微镜研究新型近 β Ti−4Al−1Sn−2Zr−5Mo−8V−2.5Cr(质量分数，%)合金经 $\alpha+\beta$ 区退火处理(ST)后进行单级时效(SA)或双级时效(DA)对显微组织演变和力学性能的影响。结果表明，与 SA 相比，合金经过 DA 处理后析出的次生 α 相更加细小，其主要机制为 300 ℃预时效形成的纳米尺度中间相 ω 颗粒可辅助次生 α 相形核，从而细化次生 α 相尺寸。另外，在一定的 ST 温度下，经 DA 处理后的合金相比于 SA 处理的合金能获得更高的强度。合金经 ST (750 ℃) + DA 后表现出优良的强度和塑性匹配，抗拉强度为 1450 MPa，伸长率为 3.87%，这主要归因于 DA 析出的纳米级次生 α 相的强化作用。可见，双级时效对新型近 β 钛合金是一种可行的热处理工艺。

关键词：新型近 β 钛合金；多向锻造；退火处理；双级时效；ω 辅助 α 形核；显微组织；力学性能

(Edited by Wei-ping CHEN)